Acta Scientific MEDICAL SCIENCES (ISSN: 2582-0931)

Volume 10 Issue 5 May 2026

Research Article

In Silico Identification of *Opuntia ficus-indica* Phytochemicals as Potential EGFR Kinase Inhibitors in Non–Small Cell Lung Cancer: Molecular Docking, Molecular Dynamics Simulation, and MM-PBSA Analyses

Mujahid M Almuqati[1]*, Rayan A Alghamdi[1] and Isam M Abu Zeid[1,2,3]

[1]Department of Biological Sciences, Faculty of Science, King Abdulaziz University, Jeddah, Saudi Arabia

[2]Centre of Excellence in Bionanoscience, King Abdulaziz University, Jeddah, Saudi Arabia

[3]Princess Dr. Najla Bint Saud Al-Saud Center for Excellence Research in Biotechnology, King Abdulaziz University, Jeddah, Saudi Arabia

***Corresponding Author:** Mujahid M Almuqati, Department of Biological Sciences, Faculty of Science, King Abdulaziz University, Jeddah, Saudi Arabia.

DOI: 10.31080/ASMS.2026.10.2237

Received: April 07, 2026

Published: May 07, 2026

Abstract

Objective: Epidermal growth factor receptor (EGFR) is a clinically validated therapeutic target in non-small cell lung cancer (NSCLC), and plant-derived phytochemicals may provide diverse lead scaffolds; thus, this study aimed to evaluate six bioactive compounds from *Opuntia ficus-indica* as potential EGFR kinase inhibitors *in silico*.

Methods: Compounds were docked into the EGFR kinase domain (PDB ID: 1XKK) using molecular docking, and the top-ranked ligands were further assessed by 100-ns molecular dynamics (MD) simulations and MM-PBSA binding free-energy calculations; the docking protocol was validated by redocking the co-crystallized ligand and computing RMSD.

Results: Docking indicated favorable accommodation within the ATP-binding pocket, with nicotiflorin (−9.43 kcal/mol), rutin (−9.11 kcal/mol), and quercetin (−8.91 kcal/mol) selected for MD/MM-PBSA, showing interactions with key ATP-site residues (e.g., Met793 and Lys745) and additional contacts including Cys797 (nicotiflorin/rutin) and Asp855 (quercetin); redocking achieved a heavy-atom RMSD of 1.268 Å, MD trajectories showed stable backbone behavior (RMSD ~0.14–0.31 nm) and maintained compactness (Rg ~1.93–2.04 nm), hydrogen-bond persistence was highest for rutin (average ~7.13; max 12) versus nicotiflorin (~4.55; max 9) and quercetin (~2.30; max 5), and MM-PBSA estimated ΔTOTAL values of −36.70 ± 5.52 (rutin), −25.58 ± 5.07 (nicotiflorin), and −23.17 ± 3.18 kcal/mol (quercetin), with favorable van der Waals/electrostatics partially offset by polar solvation and stabilized by non-polar solvation.

Conclusion: The combined docking–MD–MM-PBSA findings nominate rutin, nicotiflorin, and quercetin as the most promising *Opuntia ficus-indica* –derived EGFR-binding candidates *in silico* and support subsequent experimental validation in enzymatic and cell-based EGFR assays.

Keywords: Non-Small Cell Lung Cancer; *Opuntia ficus-indica*; Molecular Docking; Molecular Dynamics Simulation

Introduction

The identification of activating mutations in the EGFR gene established the notion of actionable changes in NSCLC and facilitated the advancement of precision medicine in lung cancer. Mutations in the tyrosine kinase domain of EGFR constitute one of the most prevalent druggable changes in NSCLC. Mutations in the EGFR kinase domain are predominantly observed in lung adenocarcinomas (LUADs), with an incidence varying between 15% and 50% according on ethnicity [1]. They are more prevalent among those with no history of smoking, females, and those of Asian descent [2,3]. In patients with NSCLC of East Asian genomic ancestry identified by a single-nucleotide variant method, the prevalence of EGFR mutations is around 50.3%, compared to 34.2%, 26.8%, 14%, and 13% for patients of South Asian, admixed American, African, and European genomic ancestries, respectively [4,5].

EGFR-mutant NSCLC constitutes a significant global health concern. The prevalence of smoking-related lung malignancies, including squamous cell carcinoma and small cell lung cancer, is declining [6]. LUAD, impacting both smokers and non-smokers, has emerged as the predominant histological subtype of lung cancer globally. LUAD is often linked to oncogenic driver mutations, including EGFR mutations, even in individuals without a history of smoking. Exposure to air pollution has been linked to a heightened incidence of lung adenocarcinomas, particularly those with EGFR mutations in non-small cell lung cancer [7].

For numerous years, researchers have concentrated on formulating novel anticancer medicines derived from plant sources [8,9]. Medicinal plants have yielded various anticancer agents utilized in therapy, including vincristine, paclitaxel, and docetaxel [8]. Both traditional and alternative medicine are employed in cancer treatment, with numerous studies indicating that medicinal plants are effective in treating lung cancer [10]. Plant extracts and their bioactive constituents have cytotoxic action by enhancing apoptosis [11–16]. Disrupting cell cycle regulation [17]. The suppression of angiogenesis [18].

Opuntia ficus-indica, a prevalent cactus species within the *Cactaceae* family, is abundant in bioactive phytochemical elements such as polyphenols, flavonoids, organic acids, amino acids, and polysaccharides [19,20]. Various plant components, including seeds, flowers, and fruits, have been acknowledged for their anticancer properties due to their cytotoxic effects on malignant cells [19]. Cladodes of Opuntia ficus-indica contain various phenols and flavonoids, including gallic acid, 3,4-dihydroxybenzoic acid, coumaric acid, 4-hydroxybenzoic acid, salicylic acid, ferulic acid, isoquercetin, nicotiflorin, isorhamnetin-3-O-glucoside, narcissin, and rutin [21]. This study aimed to investigate whether bioactive compounds derived from *Opuntia ficus-indica* can bind to the ATP-binding site of the EGFR kinase domain and to prioritize the most promising candidates by evaluating their binding suitability within the catalytic pocket, key interaction patterns with functionally important residues, the dynamic stability of the resulting complexes, and their binding energetics, thereby nominating potential starting points for subsequent experimental validation and future drug-development efforts.

Materials and Methods

Protein and ligand preparation

The crystal structure of the EGFR kinase domain (PDB ID: 1XKK) was obtained from the Protein Data Bank (https://www.rcsb.org/) (Figure 1). EGFR was chosen as the target protein due to its pivotal role in the pathogenesis of NSCLC, its frequent overexpression and activating mutations in lung tumors, and its well-established status as a clinically validated therapeutic target. The protein structure was prepared for docking using MGLTools version 1.5.7 (https://ccsb.scripps.edu/mgltools/), during which all crystallographic water molecules were removed, polar hydrogens were added, and Kollman charges were assigned. Bioactive compounds from *Opuntia ficus-indica* were retrieved from the PubChem database (https://pubchem.ncbi.nlm.nih.gov) in SDF format and subsequently converted to PDB format using Open Babel. The ligands then underwent geometric optimization and energy minimization prior to conversion into PDBQT format for docking studies.

Molecular docking

Molecular docking simulations were conducted using AutoDock Vina (v1.2.7) [22,23]. To assess the binding conformations and predicted binding affinities of the selected ligands against EGFR. The docking search region was set as a cubic grid box encompassing the ATP-binding pocket, centered at (x = 17.180, y = 33.930, z = 38.420), with dimensions of 50 × 50 × 50 Å. Docking was carried out using the following settings: exhaustiveness = 200, num_modes = 50, energy_range = 20, and min_rmsd = 0.0. The generated poses

Figure 1: A three-dimensional representation of the EGFR crystal structure was generated using Discovery Studio Visualizer.

were scored and ranked based on Vina binding energies (kcal/mol), and the highest-ranked pose for each ligand was selected for further analyses.

Validation of the docking protocol

The docking protocol was validated using a pose-reproduction (redocking) strategy based on the co-crystallized EGFR ligand. In brief, the native ligand was removed from the protein structure, and the receptor was prepared by eliminating crystallographic water molecules and non-protein heteroatoms. The receptor and native ligand were then processed separately and converted to PDBQT format using AutoDockTools. The native ligand was subsequently redocked into the EGFR ATP-binding pocket with AutoDock Vina (v1.2.7), applying the same grid configuration and docking parameters used for all screened ligands. The resulting redocked pose was superimposed onto the crystallographic conformation in PyMOL (v2.5.8), and the heavy-atom RMSD was computed. The protocol successfully recovered the native binding orientation, yielding a heavy-atom RMSD of 1.268 Å. Moreover, key protein–ligand interactions were inspected and compared using two-dimensional interaction maps generated in Discovery Studio Visualizer, confirming that the procedure reliably reproduces the native binding mode.

Molecular dynamics simulation

All MD simulations were performed on the Aziz supercomputer hosted by the high-performance computing center (HPCC) at King Abdulaziz University Jeddah, Saudi Arabia. All MD simulations were performed using GROMACS 2025.3 [24–31]. With the CHARMM36 all-atom force field and the (CHARMM-modified) TIP3P water model. Protein topology was generated using pdb2gmx. Ligands were parameterized with CGenFF by converting the selected docking poses from PDB to MOL2, generating a CHARMM stream file (.str), and converting it to GROMACS-compatible topology files using cgenff_charmm2gmx_py3_nx2.py with charmm36-jul2022.ff. Ligand coordinates were converted using gmx editconf and manually merged with the protein to generate complex.gro, while the ligand topology files (e.g., ligand.itp) were included in topol.top after verifying atom-name consistency.

Systems were solvated, neutralized, and adjusted to 0.15 M NaCl. After steepest-descent energy minimization (50,000 steps), equilibration was carried out under position restraints for 100 ps NVT at 300 K using the V-rescale thermostat ($\tau T = 0.5$ ps), followed by 100 ps NPT at 300 K and 1 bar using the C-rescale barostat ($\tau P = 5.0$ ps). Production MD was then performed for 100 ns in the NPT ensemble using the Parrinello–Rahman barostat ($\tau P = 5.0$ ps). Hydrogen-bond constraints were applied using LINCS, electrostatics were treated with PME, and short-range interactions used the Verlet scheme with 1.2 nm cutoffs (rlist = rcoulomb = rvdw = 1.2 nm). Trajectories were analyzed to compute RMSD, root mean square fluctuation (RMSF), RG, and hydrogen-bond counts.

MM-PBSA

The binding free energies (ΔG_binding) of the EGFR–ligand complexes were calculated using the MM-PBSA approach implemented in gmx_MMPBSA (v1.6.4) [32,33]. Trajectory frames were sampled from the production run at 300 K using startframe = 5001, endframe = 25001, and interval = 20, yielding a total of 1001 snapshots. Binding free energy was computed as ΔG_binding = G_complex − (G_receptor + G_ligand) and decomposed into van der Waals and electrostatic interaction energies, along with solvation contributions, where the polar solvation term was estimated using the Poisson–Boltzmann model (ipb = 2, indi = 1.0, exdi = 80.0, ionic strength = 0.15 M) and the nonpolar solvation energy was calculated using a SASA-based method (inp = 1). Entropic contributions were not included (qh_entropy = 0; interaction_entropy = 0), and results were reported as mean ± SD across all snapshots.

Results

Molecular docking of 6 phytochemicals of *Opuntia ficus-indica* against the EGFR kinase domain indicated that several ligands

could be accommodated within the ATP-binding pocket with comparable predicted affinities (Table 1). Among the screened compounds, nicotiflorin (−9.43 kcal/mol), rutin (−9.11 kcal/mol), and quercetin (−8.91 kcal/mol) yielded the most favorable docking scores; hence were chosen for subsequent binding-mode analysis and molecular dynamics simulations.

		Amino acids involved	
Ligands	**Binding affinity**	**Hydrogen binding interaction**	**Non-hydrogen interaction**
Nicotiflorin	-9.43 kcal/mol	Met793, Cys797, Lys745.	Ala743, Leu844, Leu718, Cys797, Lys745, Leu858
Rutin	-9.11 kcal/mol	Arg841, Cys797, Lys745, Asn842.	Leu844, Ala743, Leu718, Cys797, Lys745, Leu858.
Quercetin	-8.91 kcal/mol	Lys745, Thr854, Asp855, Met793.	Asp855, Lys745, Val726, Leu718, Ala743, Leu844

Table 1: Docking scores of *Opuntia ficus-indica*–derived phytochemical ligands against the receptor protein (1XKK).

Molecular interaction studies

Among the six *Opuntia ficus-indica* phytochemicals screened against the EGFR kinase domain, nicotiflorin, rutin, and quercetin produced the most favorable docking scores. Their predicted affinities were comparable, and these ligands were therefore selected for detailed binding-mode analysis. Key protein–ligand interactions within the EGFR ATP-binding pocket are summarized in Table 2 and illustrated in Figure 2a–c.

Ligand name	Compound CID	Binding affinities
Nicotiflorin	5318767	-9.43 kcal/mol
Rutin	5280805	-9.11 kcal/mol
Quercetin	5280343	-8.91 kcal/mol
Narcissin	5481663	-8.87 kcal/mol
Isorhamnetin	5281654	-8.78 kcal/mol
kaempferol	5280863	-8.70 kcal/mol

Table 2: Interaction of protein amino acid residues with ligands at receptor sites.

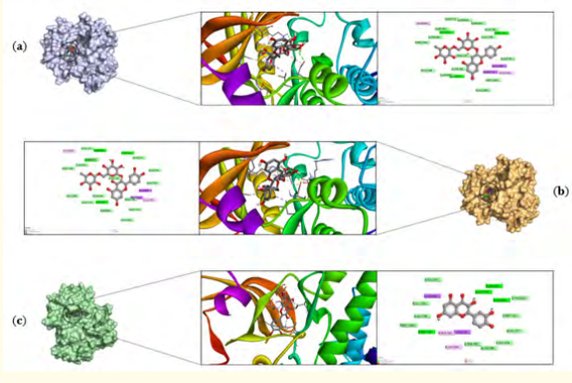

Figure 2a-c. Two-dimensional protein–ligand interaction diagrams of the top-ranked Opuntia ficus-indica phytochemicals docked into the EGFR ATP-binding site: (A) nicotiflorin, (B) rutin, and (C) quercetin. Hydrogen bonds and hydrophobic contacts are indicated in the diagrams.

Validation of docking

Cognate redocking was performed to validate the docking protocol applied to EGFR. The co-crystallized ligand was removed and subsequently redocked into the EGFR ATP-binding site using the same grid definition and docking parameters used for all screened ligands. The redocked pose was superimposed on the crystallographic conformation in PyMOL, and the similarity of the binding orientation and key protein–ligand interactions was inspected using a Discovery Studio Visualizer (Figure 3a–c). The redocked ligand closely reproduced the crystallographic pose, yielding a heavy-atom RMSD of 1.268 Å between the experimental and redocked conformations, supporting the reliability of the docking setup used in this study.

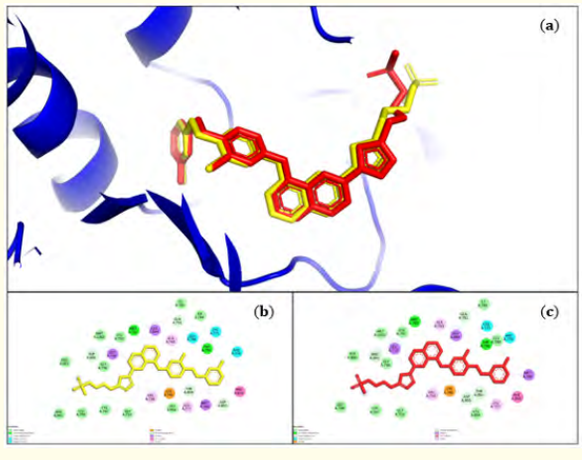

Figure 3a-c: Docking protocol validation by cognate redocking. (a) Superposition of the crystallographic pose of the co-crystallized EGFR ligand (yellow) and the redocked pose (red) within the ATP-binding site. (b) Two-dimensional interaction diagram of the crystallographic complex. (c) Two-dimensional interaction diagram of the redocked complex. The redocking reproduced the experimental binding pose with a heavy-atom RMSD of 1.268 Å.

MD simulation

This study involved the molecular dynamics simulation analysis of the crystal structure of the EGFR apo protein and its complex with chosen ligands, including emodin, aloe-emodin, and aloin, derived from docking studies. The stability of the specified protein–ligand complexes was evaluated by calculating RMSD, RMSF, RG, hydrogen bonds, and MM-PBSA throughout 100 ns for RMSD, RMSF, and RG trajectories.

The time evolution of the backbone RMSD for the apo protein and the complexes with nicotiflorin, rutin, and quercetin were monitored over 100 ns (Figure 4). All trajectories rose rapidly during the first few nanoseconds and then fluctuated within a narrow window of approximately ~0.14–0.31 nm, indicating the absence of major structural rearrangements and confirming the overall stability of the systems throughout the simulation. After equilibration (~10 ns), the apo protein fluctuated mainly between ~0.19 and 0.31 nm. The nicotiflorin-bound system showed the lowest deviations during the first half of the simulation (~0.14–0.21 nm), followed by a late increase in the second half (~0.15–0.31 nm), suggesting a conformational adjustment before reaching a stable regime. In contrast, the rutin complex exhibited comparatively restrained and consistent RMSD values (~0.17–0.28 nm) with minimal drift, while the quercetin complex remained stable (~0.17–0.31 nm) with moderate fluctuations and a slight gradual increase toward the end. Importantly, RMSD values for all systems remained well below 0.4 nm over the 100 ns trajectory.

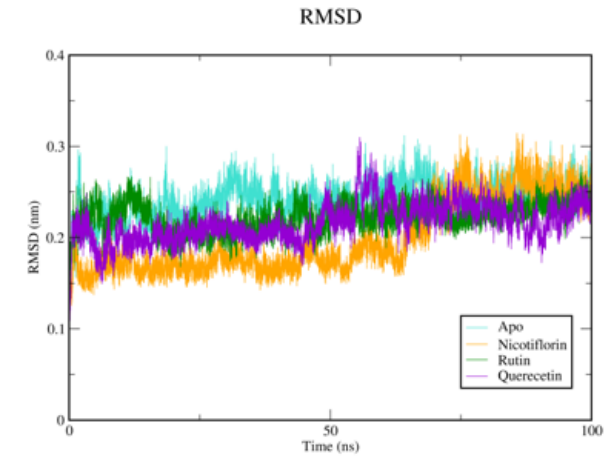

Figure 4: Time evolution of the backbone RMSD for the apo protein and the nicotiflorin, rutin, and quercetin bound complexes over the 100 ns MD simulation.

The residue-wise Cα RMSF of the apo protein and the complexes with nicotiflorin, rutin, and quercetin was evaluated over 100 ns (Figure 5). Overall, fluctuations were generally low for most residues (predominantly < ~0.15 nm), indicating a largely stable protein core, while higher mobility was confined to a few flexible segments and terminal regions. The apo protein showed relatively restrained fluctuations (approximately ~0.04–0.20 nm) with its main peak occurring around residues 995–1002 (up to ~0.28 nm). In the nicotiflorin-bound system, enhanced flexibility was observed at the N-terminal edge of the analyzed segment (residue 702; ~0.35 nm) and in two regions around residues 859–866 and 983–987, where RMSF increased to ~0.30–0.32 nm. The rutin complex displayed a comparable baseline profile but exhibited a pronounced peak at residue 702 (~0.39 nm), along with moderate increases around residues 983–987 and toward the C-terminus (up to ~0.32 nm). Notably, the quercetin complex showed the highest localized mobility, particularly near the C-terminal region (residues 1000–1003), where RMSF reached ~0.47 nm, whereas the remaining residues followed a similar low-fluctuation pattern. Collectively, the RMSF profiles suggest that ligand binding preserves the overall stability of the protein core, with differences mainly reflected in a limited number of flexible regions.

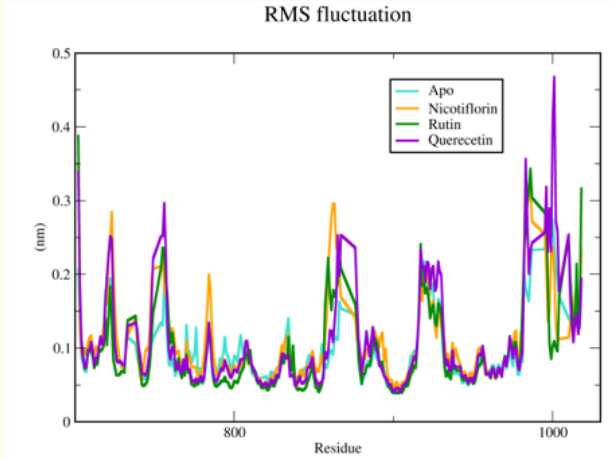

Figure 5: Residue-wise Cα RMSF of the apo protein and the nicotiflorin, rutin, and quercetin bound complexes over the 100 ns MD simulation.

The time evolution of the RG for the apo protein and the complexes with nicotiflorin, rutin, and quercetin monitored over 100 ns (Figure 6). Overall, all systems fluctuated within a

relatively narrow interval (~1.93–2.04 nm), indicating that the protein maintained a stable global compactness throughout the simulation. After equilibration (~10 ns), the apo protein remained largely stable (~1.94–2.00 nm) without noticeable drift. The rutin complex showed a similarly consistent RG profile (~1.95–2.01 nm), supporting a preserved compact fold upon binding. The quercetin complex exhibited the lowest overall RG values (~1.93–2.00 nm), suggesting a slightly more compact conformation compared with the other systems. In contrast, the nicotiflorin-bound system displayed a clear increase in RG in the second half of the trajectory (from ~1.94–2.00 nm at 10–50 ns to ~1.94–2.04 nm at 50–100 ns), consistent with a modest expansion/relaxation while remaining within a stable range.

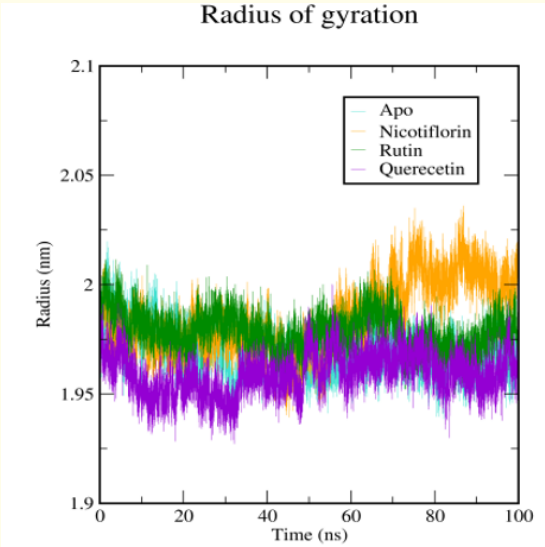

Figure 6: Time evolution of the RG of the apo protein and the nicotiflorin, rutin, and quercetin bound complexes over the 100 ns MD simulation.

Hydrogen-bond

The number of protein–ligand hydrogen bonds was monitored over 100 ns (Figure 7a-c). Overall, all complexes maintained persistent hydrogen-bond interactions throughout the trajectory, supporting stable ligand retention in the binding site. After equilibration (~10 ns), the rutin complex exhibited the highest H-bonding, with an average of ~7.13 hydrogen bonds (typically ~5–9, maximum 12), indicating the most sustained polar contacts. Nicotiflorin showed an intermediate H-bond profile (average ~4.55; typically, ~3–6; maximum 9) with a slight increase in the second half of the simulation. In contrast, quercetin formed fewer hydrogen bonds overall (average ~2.30; typically, ~1–3; maximum 5) and showed a modest reduction toward the end of the trajectory.

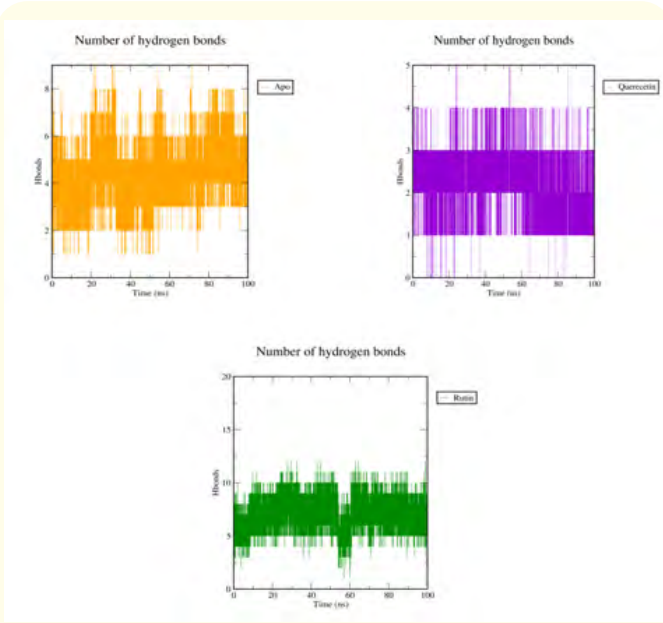

Figure 7a-c: Time evolution of the number of hydrogen bonds between the protein and (a) nicotiflorin, (b) quercetin, and (c) rutin over 100 ns of MD simulation.

MM-PBSA

Mean binding free energies for the protein–ligand systems were obtained using the gmx_MMPBSA approach. As reported in Table 3, the energy decomposition includes the van der Waals (ΔVDWAALS), electrostatic (ΔEEL), polar solvation (ΔEPB), non-polar solvation (ΔENPOLAR), and overall binding free energy (ΔTOTAL) components for the three ligands. The resulting ΔTOTAL values were −25.58 ± 5.07 kcal/mol for nicotiflorin, −23.17 ± 3.18 kcal/mol for quercetin, and −36.70 ± 5.52 kcal/mol for rutin. In general, complex formation was dominated by favorable ΔVDWAALS and ΔEEL contributions; however, these effects were partly counteracted by the ΔEPB term, whereas ΔENPOLAR remained favorable and contributed additional stabilization.

Discussion

The EGFR is a primary oncogenic driver in non-small cell lung cancer, and the ongoing issue of treatment resistance propels the

Energy Component	Nicotiflorin	Quercetin	Rutin
$\Delta_{VDWAALS\ (kcal/mol)}$	-41.29 +/- 1.73	-34.01 +/- 0.59	-49.83 +/- 1.18
$\Delta_{EEL\ (kcal/mol)}$	-58.66 +/- 2.31	-27.67 +/- 2.94	-72.28 +/- 4.87
$\Delta_{EPB\ (kcal/mol)}$	+79.58 +/- 1.52	+41.96 +/- 1.79	+91.03 +/- 2.33
$\Delta_{ENPOLAR\ (kcal/mol)}$	-5.22 +/- 0.02	-3.45 +/- 0.01	-5.63 +/- 0.05
$\Delta_{TOTAL\ (kcal/mol)}$	-25.58 +/- 3.33	-23.17 +/- 3.51	-36.70 +/- 5.57

Table 3: Binding free energy analysis of three selected complexes using MM-PBSA. Values are reported as mean ± SD (kcal/mol) over 1001 snapshots.

investigation of novel chemical scaffolds and binding mechanisms within the ATP pocket. Structural and mechanistic studies have demonstrated that EGFR activity and inhibitor response are closely associated with conformational equilibria in the kinase domain, with resistance arising from both mutational and adaptive processes that alter signaling and drug interaction [34,35].

Plants abundant in polyphenols are often investigated as sources of kinase-modulating chemotypes, with *Opuntia ficus-indica* consistently identified as a provider of flavonoids and flavonoid glycosides exhibiting various bioactivities. Analyses and compositional assessments of cladodes have identified conjugated quercetin derivatives e.g., rutin/isoquercitrin and kaempferol-rutinosides like nicotiflorin, substantiating the potential of these compounds as bioactive candidates for important biological pathways [36,37].

The interaction of canonical EGFR pocket residues at the binding-mode level corresponds with recognized principles of kinase–inhibitor recognition. Interactions in the hinge region involving Met793 are consistently emphasized as critical anchoring elements for ATP-competitive inhibitors, while adjacent residues like Lys745 often provide electrostatic stabilization. Furthermore, residues surrounding the activation segment and the aspartate–phenylalanine–glycine region, including Asp855, play a role in determining inhibitor complementarity and conformational preference [38,39].

Interactions with Cys797 are significant as this residue is a recognized pharmacological hotspot in EGFR, especially for covalent inhibitor approaches; even in non-covalent scenarios, its proximity to Cys797 may indicate advantageous positioning within the catalytic cleft. The consistency of Cys797 interaction with known inhibitor binding sites reinforces the structural validity of the docked conformations and their alignment with the well-defined architecture of the EGFR pocket [40,41].

Molecular dynamics simulation is typically utilized post-docking to assess the stability of initial poses within an explicit-solvent environment and realistic protein flexibility. The stability patterns indicated by RMSD/RMSF/Rg analyses align with expectations for well behaved kinase–ligand systems simulated using typical biomolecular engines and force fields, characterized by equilibration followed by constrained backbone deviations rather than persistent drift [42,43].

The persistence of hydrogen bonds and the distribution of local flexibility offer further mechanistic insights into the pronounced apparent engagement of glycosylated flavonoids within kinase pockets. Due to the increased density of hydrogen-bond donors and acceptors provided by sugar moieties, rutin-like scaffolds may exhibit elevated hydrogen-bond counts and improved interfacial adhesion, despite similar hydrophobic packing within a flavonoid series [44,45].

End-state free-energy rescoring MM-PBSA is frequently employed to enhance docking by integrating trajectory sampling and an implicit-solvent approach to solvation energetics; in numerous systems advantageous van der Waals/electrostatic interactions are partially counterbalanced by a polar solvation penalty, resulting in net ΔG values that more accurately represent the interaction balance in solution compared to docking scores alone. This behavior aligns with extensive methodological assessments indicating that MM-PBSA is valuable for relative

comparisons but is influenced by protocol selections and entropy management; hence, discrepancies exist between docking rank order and MM-PBSA. Rank orders are not uncommon and may indicate rescoring using an alternative physical model [46,47].

From a biological plausibility standpoint, previous experimental literature indicates that flavonoids like quercetin can influence EGFR signaling and phosphorylation in cellular environments, whereas rutin has been associated with the down regulation of EGFR/ERK axis activity, often indirectly through the regulation of upstream kinases. These studies do not independently validate direct ATP-site inhibition; rather, they reinforce the argument that engagement with the EGFR pathway is feasible for this chemical class and that computationally derived ideas regarding direct binding warrant experimental investigation [48,49].

Finally, key limitations typical of docking/MD/MM-PBSA pipelines should be considered when interpreting potency: (i) entropy is frequently omitted or approximated, (ii) results can be sensitive to protonation states and dielectric settings, and (iii) EGFR mutant landscapes e.g., resistance variants may alter pocket geometry and dynamics relative to a single crystal template. Accordingly, downstream validation is best supported by kinase assays, cellular EGFR phosphorylation readouts, and testing across clinically relevant EGFR variants to connect computed stability/ΔG trends to functional inhibition [50,51].

Conclusions

This computational investigation indicates that several *Opuntia ficus-indica* phytochemicals can be favorably accommodated within the EGFR ATP-binding pocket, with nicotiflorin, rutin, and quercetin emerging as the top docking hits (−9.43, −9.11, and −8.91 kcal/mol, respectively) and displaying binding modes that involve key catalytic/hinge-proximal residues such as Met793 and Lys745. Docking reliability was supported by successful pose reproduction of the native ligand (heavy-atom RMSD = 1.268 Å). MD simulations further supported stable complex formation over 100 ns, as reflected by bounded RMSD (~0.14–0.31 nm) and preserved compactness (RG ~1.93–2.04 nm), alongside persistent protein–ligand hydrogen bonding—particularly for rutin. MM-PBSA rescoring ranked rutin as the most favorable binder (ΔTOTAL ≈ −36.70 kcal/mol), followed by nicotiflorin and quercetin, with binding dominated by favorable van der Waals/electrostatic terms and partially offset by polar solvation. Given that entropic contributions were not included in the MM-PBSA protocol, these values should be interpreted as comparative indicators rather than absolute affinity; consequently, experimental validation EGFR kinase inhibition, cellular phosphorylation assays, and evaluation against relevant EGFR variants is warranted to confirm functional inhibition and translational potential.

Author Contributions

M.M.A. conceived and designed the study and performed molecular docking, molecular dynamics simulations, and MM-PBSA calculations, and drafted the Introduction and Methods sections. R.A.A. drafted the Results and Discussion sections, prepared the figures and tables, and contributed to interpretation of the computational findings. I.M.A.Z. substantially revised the manuscript for important intellectual content and improved the overall structure and language. All authors read and approved the final manuscript.

Funding

No external funding was received for this study.

Institutional Review Board Statement

This study did not involve human participants or animal subjects.

Informed Consent Statement

Not applicable.

Data Availability Statement

The data supporting this study are included within the manuscript.

Conflicts of Interest

The authors declare no conflicts of interest.

Bibliography

1. Tan AC., *et al*. "Targeted therapies for lung cancer patients with oncogenic driver molecular alterations". *Journal of Clinical Oncology* 40.6 (2022): 611-625.

2. Zhang YL., *et al*. "The prevalence of EGFR mutation in patients with non-small cell lung cancer: A systematic review and meta-analysis". *Oncotarget* 7.48 (2016): 78985.

3. Shi Y., *et al*. "A prospective, molecular epidemiology study of EGFR mutations in Asian patients with advanced non-small-cell lung cancer of adenocarcinoma histology (pioneer)". *Journal of Thoracal Oncology* 9.2 (2014): 154-162.

4. Adib E., *et al*. "Variation in targetable genomic alterations in non-small cell lung cancer by genetic ancestry, sex, smoking history, and histology". *Genome Medicine* 14.1 (2022): 39.

5. Miura K., *et al*. "Ancestry-, sex-, and age-based differences of gene alterations in NSCLC: From the real-world data of cancer genomic profiling tests". *JNCCN* 22.7 (2024).

6. Siegel RL., *et al*. "Cancer statistics, 2025". *CA Cancer Journal of Clinics* 75.1 (2025): 10.

7. Hill W., *et al*. "Lung adenocarcinoma promotion by air pollutants". *Nature* 616.7955 (2023): 159-167.

8. Marmitt DJ., *et al*. "Renisus plants and their potential antitumor effects in clinical trials and registered patents". *Nutritional Cancer* 73.10 (2021): 1821-1848.

9. Yurt Kilcar A., *et al*. "In vitro evaluation of radiolabeled (125I) methanol extracts of yarrow in cell lines of MCF-7, PC-3, A-549 and Caco-2". *Journal of Radioanalytical and Nuclear Chemistry* 295.1 (2012): 593-599.

10. Memarzia A., *et al*. "Therapeutic effects of medicinal plants and their constituents on lung cancer, in vitro, in vivo and clinical evidence". *Journal of Cellular and Molecular Medicine* 27.19 (2023): 2841-2863.

11. Zhiyuan HU., *et al*. "Hyperoside exhibits anticancer activity in non small cell lung cancer cells with T790M mutations by upregulating FoxO1 via CCAT1". *Oncology Report* 43.2 (2020): 617-624.

12. Qu H., *et al*. "Structural characterization of a polysaccharide from the flower buds of Tussilago farfara, and its effect on proliferation and apoptosis of A549 human non-small lung cancer cell line". *International Journal of Biological Macromolecules* 113 (2018): 849-858.

13. Yu PP., *et al*. "Millifolide a, a dimeric ether of degraded sesquiterpene lactones, inhibited the proliferation of human lung cancer cell line A549". *Natural Product Research* 36.11 (2022): 2875-2877.

14. Chen WT., *et al*. "Hyperforin suppresses tumor growth and NF-κB-mediated anti-apoptotic and invasive potential of non-small cell lung cancer". *Anticancer Research* 38.4 (2018): 2161-2167.

15. Taşkonak B., *et al*. "Hypericin-loaded chitosan nanoparticles for enhanced photodynamic therapy in A549 lung cancer cells". *BioNanoScience* 13.2 (2023): 352-364.

16. Zhu L hua., *et al*. "Cycloastragenol induces apoptosis and protective autophagy through AMPK/ULK1/mTOR axis in human non-small cell lung cancer cell lines". *Journal of Integrative Medicine* 22.4 (2024): 503-514.

17. Qu H., *et al*. " Structural characterization of a polysaccharide from the flower buds of Tussilago farfara, and its effect on proliferation and apoptosis of A549 human non-small lung cancer cell line". *International Journal of Biological Macromolecules* 113 (2018): 849-858.

18. Memarzia A., *et al*. "Therapeutic effects of medicinal plants and their constituents on lung cancer, in vitro, in vivo and clinical evidence". *Journal of Cellular and Molecular Medicine* 27.19 (2023): 2841-2863.

19. Nam DG., *et al*. "The cactus (Opuntiathecus-indica) cladodes and callus extracts: A study combined with LC-MS metabolic profiling, in-silico, and in-vitro analyses". *Antioxidants* 12.7 (2023): 1329.

20. Alholy T., *et al*. "Biosynthesis of magnesium oxide nanoparticles using Opunita ficus-indica and their antifungal effect against Aspergillus niger". *Journal of Research in Pharmacy* 27.3 (2023): 1188-1201.

21. El-Mostafa K., *et al*. "Nopal cactus (Opuntia ficus-indica) as a source of bioactive compounds for nutrition, health and disease". *Molecules* 19.9 (2014): 14879-14901.

22. Trott O., *et al*. "Autodock vina: Improving the speed and accuracy of docking with a new scoring function, efficient optimization, and multithreading". *Journal of Computational Chemistry* 31.2 (2010): 455-461.

23. Eberhardt J., *et al*. "Autodock vina 1.2.0: New docking methods, expanded force field, and python bindings". *Journal of Chemical Information and Modeling* 61.8 (2021): 3891-3898.

24. Bekker H., *et al*. "Gromacs-a parallel computer for molecular-dynamics simulations in 4th international conference on computational physics (PC 92)". *WSPC* (1993): 252-256.

25. Berendsen HJC., *et al*. "Gromacs: A message-passing parallel molecular dynamics implementation". *Computer Physics Communications* 91.1-3 (1995): 43-56.

26. Lindahl E., *et al*. "Gromacs 3.0: A package for molecular simulation and trajectory analysis". *Journal of Molecular Modeling* 7.8 (2007): 306-317.

27. Van Der Spoel D., *et al*. "Gromacs: Fast, flexible, and free". *Journal of Computational Chemistry* 26.16 (2006): 1701-1718.

28. Hess B., *et al*. "Gromacs 4: Algorithms for highly efficient, load-balanced, and scalable molecular simulation". *Journal of Chemical Theory and Computation* 4.3 (2008): 435-447.

29. Pronk S., *et al*. "Gromacs 4.5: A high-throughput and highly parallel open-source molecular simulation toolkit". *Bioinformatics* 29.7 (2013): 845-854.

30. Páll S., *et al*. "Tackling exascale software challenges in molecular dynamics simulations with gromacs". *Lecture Notes in Computer Science LNCS* 8759 (2015): 23-27.

31. Abraham MJ., *et al*. "Gromacs: High performance molecular simulations through multi-level parallelism from laptops to supercomputers". *Software X* 1-2 (2015): 19-25.

32. Miller BR., *et al*. "MMPBSA.py: An efficient program for end-state free energy calculations". *Journal of Chemical Theory and Computation* 8.9 (2012): 3314-3321.

33. Valdés-Tresanco MS., *et al*. "gmx_MMPBSA: A new tool to perform end-state free energy calculations with gromacs". *Journal of Chemical Theory and Computation* 17.10 (2021): 6281-6291.

34. Roberts SK., *et al*. "Targeting mutant EGFR in non-small cell lung cancer in the context of cell adaptation and resistance". *Drug Discovery Today* 30.7 (2025): 104407.

35. Galdadas I., *et al*. "Structural basis of the effect of activating mutations on the EGF receptor". *Elife* 10 (2021).

36. Rocchetti G., *et al*. "Italian Opuntia ficus-indica cladodes as rich source of bioactive compounds with health-promoting properties". *Foods* 7.2 (2018): 24.

37. El-Mostafa K., *et al*. "Nopal cactus (Opuntia ficus-indica) as a source of bioactive compounds for nutrition, health and disease". *Molecules* 19.9 (2014): 14879-14901.

38. de Oliveira TA., *et al*. "Evaluation of docking machine learning and molecular dynamics methodologies for DNA-ligand systems". *Pharmaceuticals* 15.2 (2022): 132.

39. Trott O., *et al*. "Autodock vina: Improving the speed and accuracy of docking with a new scoring function, efficient optimization and multithreading". *Journal of Computational Chemistry* 31.2 (2010): 455.

40. Roberts SK., *et al*. "Targeting mutant EGFR in non-small cell lung cancer in the context of cell adaptation and resistance". *Drug Discovery Today* 30.7 (2025): 104407.

41. Amelia T., *et al*. "Structural insight and development of EGFR tyrosine kinase inhibitors". *Molecules* 27.3 (2022): 819.

42. Patil BR., *et al*. "Exploring the structural activity relationship of the osimertinib: A covalent inhibitor of double mutant EGFRL858R/T790M tyrosine kinase for the treatment of non-small cell lung cancer (NSCLC)". *Bioorganic and Medicinal Chemistry* 109 (2024).

43. Amelia T., *et al*. "Structural insight and development of EGFR tyrosine kinase inhibitors". *Molecules* 27.3 (2022): 819.

44. Huang J., *et al*. "CHARMM36 all-atom additive protein force field: Validation based on comparison to NMR data". *Journal of Computational Chemistry* 34.25 (2013): 2135-2145.

45. Abraham MJ., *et al*. "Gromacs: High performance molecular simulations through multi-level parallelism from laptops to supercomputers". *SoftwareX* 1-2 (2015): 19-25.

46. El-Mostafa K., *et al*. "Nopal cactus (Opuntia ficus-indica) as a source of bioactive compounds for nutrition, health and disease". *Molecules* 19.9 (2014): 14879-901.

47. Rocchetti G., *et al*. "Italian Opuntia ficus-indica Cladodes as Rich Source of Bioactive Compounds with Health-Promoting Properties". *Foods* 7.2 (2018): 24.

48. Valdés-Tresanco MS., *et al*. "gmx_MMPBSA: A new tool to perform end-state free energy calculations with gromacs". *Journal of Chemical Theory and Computation* 17.10 (2021): 6281-6291.

49. Genheden S., *et al*. "The MM/PBSA and MM/GBSA methods to estimate ligand-binding affinities". *Expert Opinion on Drug Discovery* 10.5 (2015): 449.

50. Liu Y., *et al*. "Quercetin attenuates podocyte apoptosis of diabetic nephropathy through targeting EGFR Signaling". *Frontiers in Pharmacology* 12 (2022): 792777.

51. Huang YT., *et al*. "Effects of luteolin and quercetin, inhibitors of tyrosine kinase, on cell growth and metastasis-associated properties in A431 cells overexpressing epidermal growth factor receptor". *British Journal of Pharmacology* 128.5 (1999): 999-1010.

52. Galdadas I., *et al*. "Structural basis of the effect of activating mutations on the EGF receptor". *Elife* 10 (2025).

53. Genheden S., *et al*. "The MM/PBSA and MM/GBSA methods to estimate ligand-binding affinities". *Expert Opinion on Drug Discovery* 10.5 (2015): 449.